doi:10.1006/jmbi.2002.5442 available online at http://www.idealibrary.com on IDEAL® J. Mol. Biol. (2002) 317, 697–706

JMB

Localization of Uroplakin Ia, the Urothelial Receptor for Bacterial Adhesin FimH, on the Six Inner Domains of the 16 nm Urothelial Plaque Particle

Guangwei Min[1], Martin Stolz[2], Ge Zhou[1], Fengxia Liang[3], Peter Sebbel[4] Daniel Stoffler[5], Rudi Glockshuber[4], Tung-Tien Sun[3], Ueli Aebi[2] and Xiang-Peng Kong[1]*

[1]*Structural Biology Program Skirball Institute of Biomolecular Medicine Department of Biochemistry New York University School of Medicine New York, NY 10016 USA*

[2]*M. E. Müller Institute for Structural Biology, Biozentrum University of Basel, CH-4056, Basel, Switzerland; and*

[3]*Departments of Dermatology Pharmacology and Urology New York University School of Medicine, New York, NY 10016, USA*

[4]*Institut für Molekularbiologie und Biophysik, Eidgenössische Technische Hochschule Hönggerberg, CH-8093 Zürich Switzerland*

[5]*The Scripps Research Institute La Jolla, CA 92307, USA*

**Corresponding author*

The binding of uropathogenic *Escherichia coli* to the urothelial surface is a critical initial event for establishing urinary tract infection, because it prevents the bacteria from being removed by micturition and it triggers bacterial invasion as well as host cell defense. This binding is mediated by the FimH adhesin located at the tip of the bacterial type 1-fimbrium and its urothelial receptor, uroplakin Ia (UPIa). To localize the UPIa receptor on the 16 nm particles that form two-dimensional crystals of asymmetric unit membrane (AUM) covering >90 % of the apical urothelial surface, we constructed a 15 Å resolution 3-D model of the mouse 16 nm AUM particle by negative staining and electron crystallography. Similar to previous lower-resolution models of bovine and pig AUM particles, the mouse 16 nm AUM particle consists of six inner and six outer domains that are interconnected to form a twisted ribbon-like structure. Treatment of urothelial plaques with 0.02-0.1 % (v/v) Triton X-100 allowed the stain to penetrate into the membrane, revealing parts of the uroplakin transmembrane moiety with an overall diameter of 14 nm, which was much bigger than the 11 nm value determined earlier by quick-freeze deep-etch. Atomic force microscopy of native, unfixed mouse and bovine urothelial plaques confirmed the overall structure of the luminal 16 nm AUM particle that was raised by 6.5 nm above the luminal membrane surface and, in addition, revealed a circular, 0.5 nm high, cytoplasmic protrusion of ~14 nm diameter. Finally, a difference map calculated from the mouse urothelial plaque images collected in the presence and absence of recombinant bacterial FimH/FimC complex revealed the selective binding of FimH to the six inner domains of the 16 nm AUM particle. These results indicate that the 16 nm AUM particle is anchored by a ~14 nm diameter transmembrane stalk, and suggest that bacterial binding to UPIa that resides within the six inner domains of the 16 nm AUM particle may preferentially trigger transmembrane signaling involved in bacterial invasion and host cell defense.

Keywords: asymmetric unit membrane; bladder epithelium; uroplakin; urinary tract infection; bacterial adhesin

Introduction

The apical surface of mammalian bladder epithelium is highly specialized, as it is composed almost entirely of rigid-looking plaques, known as urothelial plaques or asymmetric unit membranes (AUM), that are typically 0.2-1 μm in diameter and consist of 2-D crystals of hexagonally packed 16 nm protein particles.[1–5] It has been suggested

Abbreviations used: AUM, asymmetric unit membrane(s); AFM, atomic force microscopy; EM, electron microscope(y).

E-mail address of the corresponding author: kong@saturn.med.nyu.edu

0022-2836/02/050697–10 $35.00/0

that these plaques contribute to the remarkable permeability barrier function of the urothelium, to the reversible adjustment of the apical surface area, and to the physical stabilization of the apical surface during bladder distention.[6,7] In addition, binding of uropathogenic bacteria to these plaques enables them to establish an infection by triggering bacterial invasion and urothelial host-cell defense mechanisms.[8] Hence, it is evident that urothelial plaques play a pivotal role in many urothelial functions and urological diseases, including urinary tract infection.

Using negative staining and image processing, we and others have shown that the 16 nm AUM particles, which are exposed on the luminal side of urothelial plaques, can be resolved into six inner and six outer domains that are interconnected to form a twisted ribbon-like structure.[9] The cytoplasmic face of urothelial plaques appeared smooth and structureless, leading to an early suggestion that the protein subunits of urothelial plaques are ''floating'' on the surface of the lipid bilayer without having a transmembrane anchor.[10] Recent data showed, however, that the 16 nm AUM particles of bovine urothelial plaques are composed of four major integral membrane proteins, i.e. uroplakins Ia (27 kDa), Ib (28 kDa), II (15kda) and III (47 kDa) that all possess transmembrane domains.[6] Uroplakins Ia and Ib are ~38 % identical. They belong to a gene family called tetraspanins that includes CD37, CD63 and CD81, and they all span the membrane four times.[11,12] On the other hand, UPII and III possess only a single transmembrane domain, and they share a stretch of ~12 amino acid residues located juxtamembrane on the extracellular side.[13-15] With the exception of UPIII, which has a relatively long cytoplasmic domain of ~50 amino acid residues, all major hydrophilic loops of uroplakins are extracellular, aggregating tightly with one another to form the 16 nm AUM particle.[16] The four uroplakins can be divided into two pairs consisting of UPIa/UPII and UPIb/UPIII, because: (i) UPIa and UPIb were found to crosslink to UPII and UPIII, respectively;[17] (ii) complexes of UPIa/UPII and UPIb/UPIII can be separated by ion-exchange chromatography;[18] and (iii) ablation of the mouse UPIII gene selectively perturbed the glycosylation and targeting of its putative partner UPIb.[19] Overall, there is no doubt that uroplakins play a key role in urothelial functions, because uroplakins are synthesized as major urothelial specialization products in a urothelium-specific and differentiation-dependent manner, and because 2-D crystals of uroplakins cover almost the entire apical urothelial surface.[6] Before we can begin to understand how uroplakins perform their functions, however, we must first know how these integral membrane proteins interact with one another, and how such interactions may be regulated. Therefore, the localization of individual uroplakins within the 16 nm AUM particles represents a critical initial step towards a rational understanding of urothelial function.

The urothelial receptor for the uropathogenic bacterium *Escherichia coli*, which causes over 85 % of all urinary tract infections, has been identified recently to be uroplakin Ia.[20] FimH is the bacterial adhesin located at the tip of the type 1 fimbria of *E. coli*, and is known to bind to the high-mannose sugar moieties of the urothelial receptor.[20-23] Wu *et al*. found that ^{35}S-methionine-labeled type 1-fimbriated *E. coli*, when incubated with urothelial plaque proteins that had been resolved by SDS-PAGE and transferred to nitrocellulose paper, bound to two bands of ~24 kDa and ~27 kDa, which were thought to represent UPIa and UPIb.[17] The precise identification of bovine UPIa (27 kDa) and UPIb (28 kDa) has been difficult, however, because they are resolved only partially by SDS-PAGE. By studying mouse urothelial plaques whose UPIa (24 kDa) and UPIb (28 kDa) are much better resolved, we have shown recently that both radiolabeled *E. coli* and biotinylated recombinant FimH (the latter having been prepared as a complex with its stabilizing chaperone FimC) bind selectively to UPIa, and that the bovine duplex previously detected most likely represent UPIa and a UPIa degradation product.[20]

The identification of UPIa as the major FimH receptor has important implications for the mechanisms of bacterial:urothelial host cell interaction, and for the ultrastructural localization of uroplakin Ia. We have previously prepared a panel of antibodies to synthetic peptides corresponding to a number of domains of UPIa as well as other uroplakins.[18] Although these antibodies work well for immunoblotting, many of them yielded weak signals when used for immunohistochemical staining or immuno-gold electron microscope (EM) localization, probably due to the inaccessibility of the epitopes that are buried in the tightly packed 16 nm AUM particle structure. In contrast, FimH works well for immunohistochemical staining, probably reflecting the fact that sugar moieties are usually exposed on the protein surface. The availability of milligram quantities of highly purified recombinant FimH/FimC complex therefore offers unique opportunities for the direct tagging and thereby the localization of uroplakin Ia within the 16 nm AUM particle.[20,24–26]

Most of the previous structural studies of the 16 nm AUM particle have been performed using bovine and pig urothelial plaques, yielding 3-D reconstructions at about 22 Å resolution.[9,27,28] We have decided, however, to carry out our present studies using mainly mouse urothelial plaques, for several reasons. First, better quality and larger crystalline plaques can be isolated from mouse bladders, which we can obtain much more freshly than the slaughterhouse materials, thus resulting in higher resolution. Second, structural information of the mouse urothelial plaques may be more biologically relevant because mouse bladder has been used routinely as models for studying urothelial physiology, urinary tract infection,[8] bladder cancer formation[29,30] and, more recently, certain heredi-

tary urological diseases by the gene knockout approach.[19]

Hence, we have performed a 3-D reconstruction of negatively stained mouse AUM particles at a nominal resolution of 15 Å. The resulting model revealed that the structure of the mouse AUM particle was similar to that of other species, i.e. consisting of six inner and six outer domains interconnected to yield a twisted ribbon-like structure thus providing additional support to the idea that uroplakin structure is highly conserved during mammalian evolution. Atomic force microscopy (AFM) of fully native, i.e. unfixed/unstained mouse and bovine urothelial plaques confirmed the overall configuration of the AUM particle structure and, in addition, revealed for the first time a circular, 0.5 nm high, cytoplasmic protrusion. Finally, by calculating a Fourier space difference map of the AUM particle in the presence and absence of recombinant FimH/FimC complex, we showed that the bacterial adhesin binds selectively to the six inner domains of the 16 nm AUM particle. These results show that the high mannose sugar moieties of uroplakin Ia are associated with the inner domains of the AUM particle, and suggest that, upon bacterial binding, such domains may be preferentially involved in transmitting signals into the cytoplasm thereby triggering bacterial invasion and host cell defense.

Results

A 3-D reconstruction of mouse AUM particle at 15 Å resolution

To study the fine structure of mouse urothelial plaques, we isolated crude membranes from mouse bladders using discontinuous sucrose density-gradient centrifugation, followed by washing the membranes using 2% (v/v) Sarkosyl, which removed the contaminating non-plaque membrane proteins. Such highly purified urothelial plaques (yield ~0.1 mg per mouse bladder)[31,32] contained mainly the four uroplakins (see below), and appeared quite homogeneous, as seen by electron microscopy (Figure 1(a)). A significant number of plaques were as large as 0.7-1 μm in diameter (Figure 1(a)); only rarely did we see isolated bovine plaques of such a large size. Thus, the calculated diffraction patterns of mouse plaques (Figure 1(b))

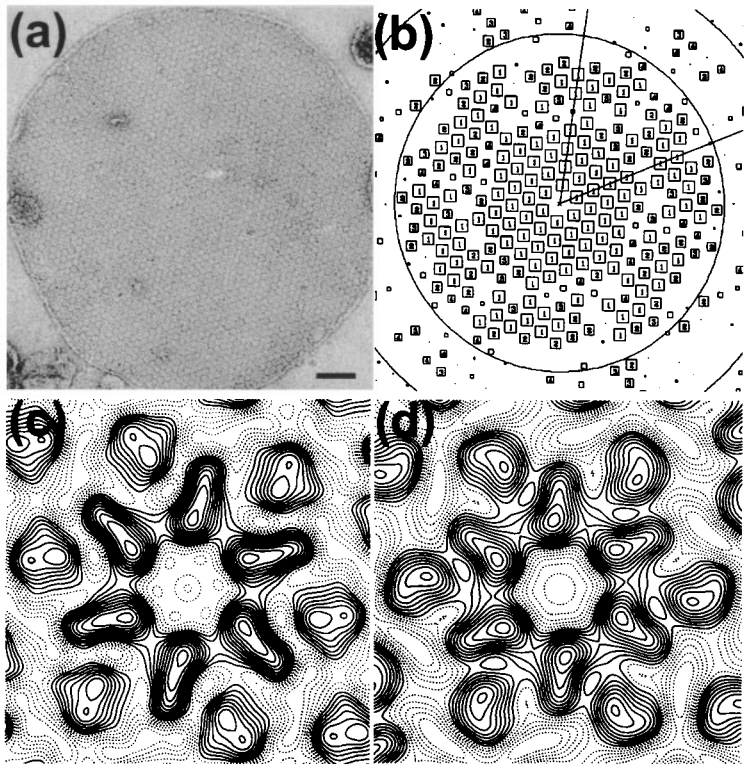

Figure 1. Electron microscopy and 2-D projection map of urothelial plaques. (a) An isolated mouse AUM plaque that was negatively stained with 0.75% uranyl formate. The scale bar represents 100 nm. (b) The calculated diffraction pattern of a negatively stained mouse urothelial plaque (~1 μm diameter). Each spot with a signal to noise ratio of >1 is shown as a square; the size of the square is proportional to the signal to noise ratio. The number in each square represents the IQ number of the diffraction spot ($IQ = 1$ and $IQ = 7$ correspond to signal-to-noise ratio of 7 and 1, respectively).[42] Circles are drawn at contrast transfer function (CTF) correction zeros and the first circle corresponds to approximately 15 Å. Note many spots with a resolution of better than 15 Å. (c) A 2-D project map of a mouse urothelial plaque at ~15 Å resolution. (d) A 2-D projection map of a bovine urothelial plaque at ~20 Å resolution.

were superior to those of the bovine plaques, allowing the calculation of a mouse AUM project map at 15 Å resolution (Figure 1(c)). Comparison of this map with that of the bovine plaque (Figure 1(d) at 20 Å resolution) showed that each mouse AUM particle, like the bovine, consisted of six inner and six outer domains.[9,27,28,33,34] However, the higher-resolution map of mouse AUM particle revealed that the six outer domains were less connected to the six inner domains than previously thought, and that each outer domain could be further divided into two smaller subdomains (Figure 1(c)).

To study the 3-D structure of the mouse 16 nm AUM particle, we recorded a tilt series (41 images) of negatively stained AUM plaques at 0°, 20° 30° 45° and 55° in low-dose mode, and computed a 3-D density map to the resolution of 15 Å (overall weighted phase error at 19.7°; Figure 2(b)-(d) and Table 1). The luminal portion of the AUM particle had six inner domains and six outer domains connected together forming a twisted ribbon-like

Table 1. Parameters of the 3-D reconstruction

Parameter	Value
Number of images	41
Unit cell parameters a, b(Å), γ (deg.)	165, 165, 120
Two-sided plane group	P_6
Range of underfocus (Å)	−3000 to −20,000
Range of crystal tilts (deg.)	0 to 55
Overall weighted phase residual (deg.)	19.7
Resolution cutoff (Å)	15

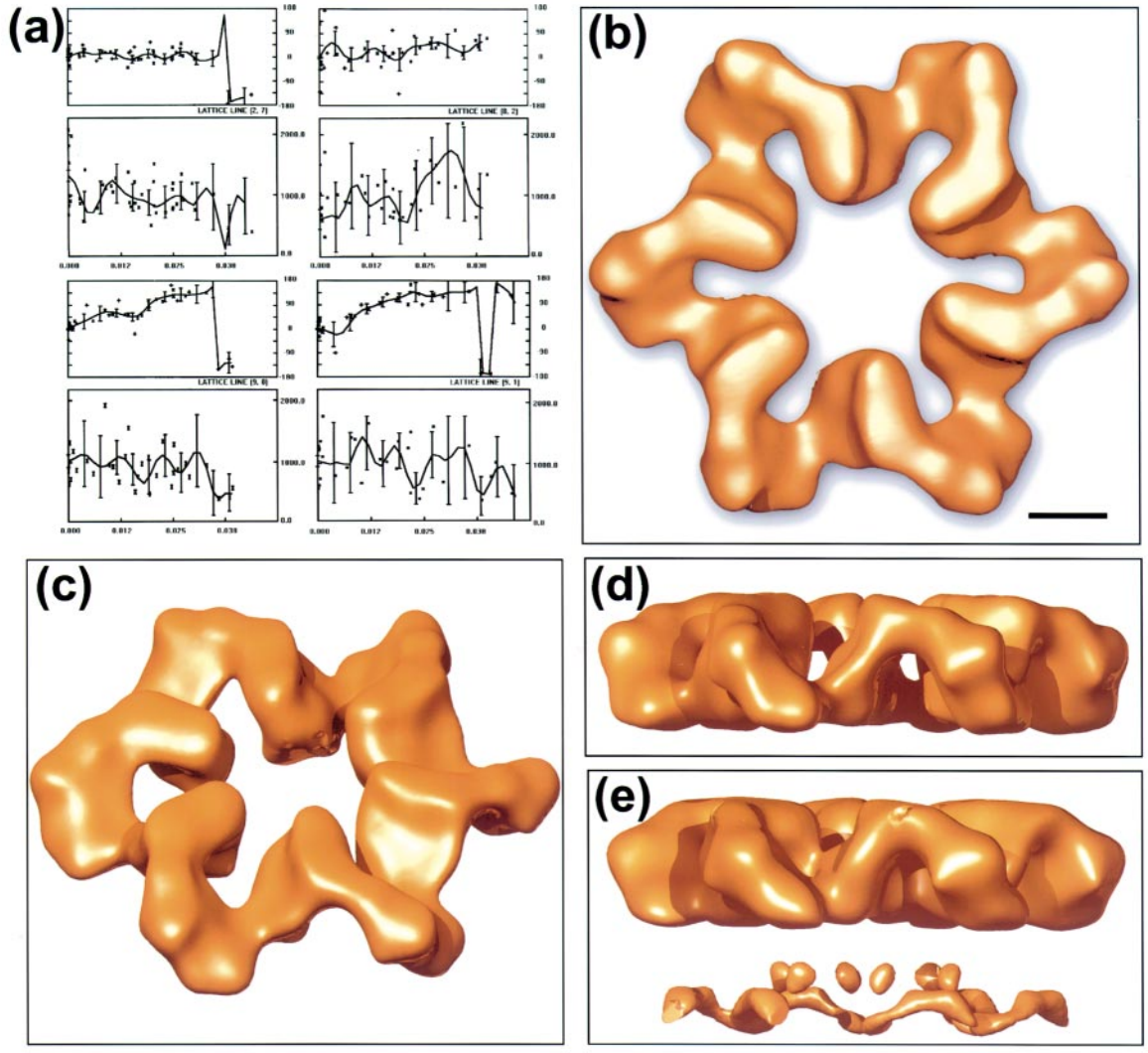

Figure 2. Three-dimensional reconstruction of the mouse 16 nm AUM particle. (a) The phase and amplitude variations along some of the high-resolution lattice lines after merging data from the tilted plaques in the two-sided plane space group P_6. The points included all the data with $IQ < 6$. The curves were computed using the LATLINE program from the MRC software suite.[46] (b)-(d) The top view, a 45° tilted view, and the side-view of a mouse AUM particle. (e) A side-view of a mouse 16 nm AUM particle in plaques that had been treated with 0.02% Triton X-100; note the partial visualization of the transmembrane moiety. (b) The scale bar represents 2.5 nm.

structure (Figure 2(b)).[9] The diameter of the AUM particle is ~17.0 nm, with a central hole that is ~4.5 nm in diameter (Figure 2(b) and (c)).

Partial visualization of the transmembrane portion of the AUM particles

To determine which side of the 3-D image was in direct contact with the lipid bilayer, we treated the mouse urothelial plaques with various concentrations of Triton X-100 which, by partially removing the lipids, enabled the ionic stains to penetrate into the lipid bilayer, thus revealing some of the transmembrane moieties. We found that while a high concentration of Triton X-100 (>0.2 %, v/v) destroyed the plaque structure, consistent with the earlier results,[31,32] low concentrations of the detergent (0.02 to 0.1 %) revealed some intramembranous moieties (Figure 2(e)), thus enabling us to orient the AUM particle with respect to the lipid bilayer. The data indicated that the partially revealed transmembrane moiety occupied an area that was ~14 nm in diameter, which is significantly larger than the 11 nm value we obtained earlier from quick-freeze deep-etch studies (Figure 2(e); also see below).

Visualization of fully native mouse and bovine urothelial plaques by AFM

We next used AFM, which was particularly suitable for studying the surface topographies of native biomembrane,[35] to examine the luminal and cytoplasmic surfaces of mouse and bovine urothelial plaques. As documented in Figure 3(a) and (b), the luminal surface of the AUM plaque was characterized by hexagonal arrays of 16 nm AUM particles, which had an overall configuration very similar to that revealed by transmission EM of negatively stained specimens, thus confirming the validity of the negative-staining data (compare Figure 3(a) and (b) with Figure 1(a)). The similarity between the AFM and the EM data becomes even more evident when one superimposes and aligns the two images (Figure 4) using ViPEr, a novel platform-independent visual-programming environment based on Python, Tkinter and OpenGL. (M.F. Sanner, D.S., & A.J. Olson, unpublished results) This comparison clearly documented that the tip of the negatively stained 16 nm AUM particle was flattened compared with the AFM image, most likely due to drying.

Although the cytoplasmic surface of AUM was thought to be flat and featureless, AFM revealed, for the first time, arrays of circular, ~0.5 nm high protrusions that were ~14 nm in diameter (Figure 3(c), (d), and (e) lower right half). Most likely, these relatively flat circular cytoplasmic protrusions corresponded to the transmembrane moiety of the AUM particles that were seen after the urothelial plaques were subjected to a ''mild'' Triton treatment (cf. Figure 2(e)). Although the luminal surface topography of mouse (Figure 3(a) and (b)) and bovine (data not shown) AUM plaques were indistinguishable in their image quality, the cytoplasmic image of mouse AUM plaques was inferior to that of bovine plaques (Figure 3(c) and (d), and data not shown).

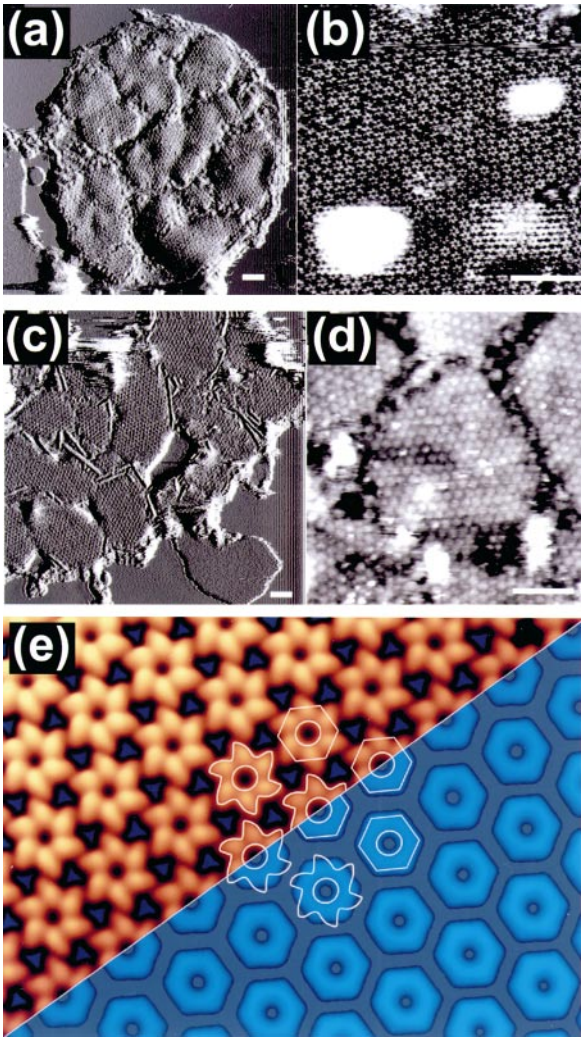

Figure 3. Visualization of mouse and bovine urothelial plaques by atomic force microscopy. (a) Low magnification view of the luminal face of several bovine urothelial plaques. (b) High-magnification view of the luminal surface of a bovine urothelial plaque. Note the hexagonally packed 16 nm AUM particles that could be readily visualized even without averaging. (c) Low-magnification view of the cytoplasmic face of several bovine urothelial plaques. (d) High-magnification view of the cytoplasmic face of several bovine urothelial plaques. Note the presence of rather flat, donut-like protrusions. (e) The averaged images of the luminal (upper left half in red) and cytoplasmic (lower right half in blue) surfaces of bovine and mouse, respectively, urothelial plaques. Note the propeller-shaped 16 nm AUM particles on the luminal surface, and the ~14 nm diameter, circular protrusions on the cytoplasmic surface. The scale bars in (a)-(d) represent 100 nm.

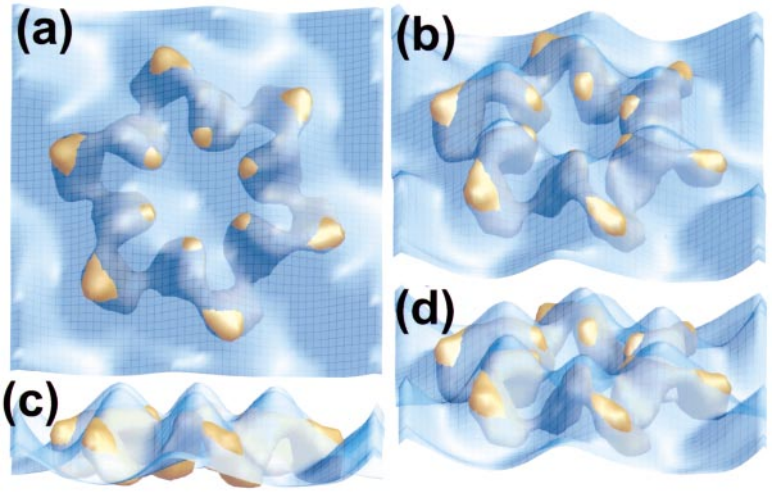

Figure 4. Comparison of the surface topolography of urothelial 16 nm AUM particle as defined by negative staining and atomic force microscopy (AFM). The negative stained 3-D reconstruction of a 16 nm mouse AUM particle (yellow) and the surface topolography of a mouse luminal urothelial plaque obtained by AFM (blue) were superimposed, and shown from (a) the top, (c) side or (b) and (d) from two other intermediate angles. For better comparison, the AFM surface is rendered transparent and a grid mesh of the same surface is put on top of it. Note the overall consistency of the negative staining and AFM data. The negatively stained particle was flatter than the AFM-defined particle. This discrepancy is particularly evident in (c) the side view, most likely due to drying artifacts of the EM specimen.

The binding of FimH to isolated mouse urothelial plaques

To localize uroplakin Ia in the 16 nm AUM particle, we mapped the FimH binding site on the 16 nm AUM particle of mouse urothelial plaques using a complex of recombinant FimH and FimC. We used this complex for localization because FimC, which does not affect the binding of FimH to its mannose ligand, protects FimH from degradation,[36] and because this is the same complex that we showed earlier to bind specifically to uroplakin Ia (Figure 5(a))[20]. We constructed a difference map using the method of Kubalek *et al*. by first calculating the difference of the scaled structure factors between the native (without FimH/FimC; 14 micrographs; phase residual 17.3°) and derivative (with FimH/FimC; 17 micrographs; phase residual 19.8°) followed by calculating the differences using the native phases.[37] This map revealed a single positive peak corresponding to the six inner domains of the AUM particle (see Figure 5(b) for the 2-D projection map and Figure 5(c) for the 3-D model).

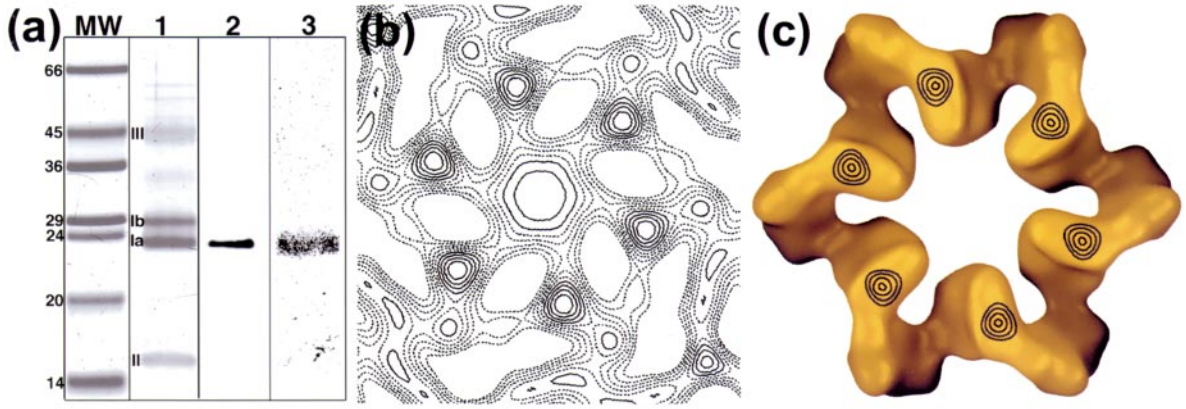

Figure 5. Localization of uroplakin Ia receptor of the bacterial FimH on the six inner domains of the mouse 16 nm AUM particle. (a) The UPIa specificity of the FimH/FimC complex. Recombinant FimH/FimC complex was biotinylated and incubated with mouse urothelial plaque proteins that had been resolved by SDS-PAGE and transferred to a nitrocellulose membrane. (1) Total proteins of mouse urothelial plaque visualized by Coomassie blue staining showing the separation of uroplakin II (15 kDa), UPIa (24 kDa), UPIb (27 kDa) and UPIII (47 kDa); note the excellent resolution between uroplakins Ia and Ib. (2) Selective binding of FimH/FimC to uroplakin Ia. (3) Selective binding of ^{35}S-methionine-labeled type 1-fimbriated *E. coli* to uroplakin Ia. MW: molecular mass standards. (b) A 2-D difference map of the mouse urothelial plaque images collected in the presence and absence of FimH/FimC. (c) The localization of the FimH binding site when projected onto the 3-D model of the 16 nm AUM particle. Note the association of FimH with the six inner domains of the 16 nm AUM particle.

Discussion

We have established here that the structure of the mammalian urothelial plaques is highly conserved (Figure 1). Moreover, we have visualized for the first time parts of the transmembrane moiety of the 16 nm AUM particle (Figure 2(e)) and their corresponding protrusions on the cytoplasmic surface of urothelial plaques (Figure 3). Most importantly, we have localized uroplakin Ia, the FimH receptor, on the six inner domains of the 16 nm AUM particle (Figure 5).

The 3-D structure of urothelial plaques is highly conserved

Previous studies have indicated that urothelial plaques are highly conserved structurally. For example, early studies of negatively stained urothelial plaques using EM revealed similar hexagonal arrays of 16 nm AUM particles, each consisting of six inner and six outer domains, for rat,[38] pig,[27] and for mouse, rat and monkey.[39] The 3D models of pig and bovine AUM particles revealed that the 12 domains are interconnected, forming a twisted ribbon-like structure.[9,27,28] We show here that the 3-D reconstruction of mouse AUM particle adopts a structure almost identical with that of the bovine AUM particle (Figures 1 and 2). The remarkable conservation of the AUM structure is consistent with the fact that uroplakins, i.e. the major molecular building blocks of urothelial plaques, appear highly conserved biochemically and immunologically[6,39]. Such a strict conservation of urothelial plaque structure during mammalian evolution suggests strongly that the characteristic structural features of urothelial plaques must serve critically important biological functions.

Gathering detailed structural information on urothelial plaques using various imaging techniques, including EM and AFM, is crucial to our eventual understanding of uroplakin function, their molecular interactions, and their supramolecular assemblies. However, a given method either provides only partial insight or is subject to preparative experimental artifacts, due to the size and complexity of the molecular system under investigation. Here, we present for the first time a combination of 3-D electron density data from EM of negatively stained 16 nm particles and surface information from AFM of the apical membrane kept in buffer. As shown in Figure 4, the two sets of data correlate very well, although the negatively stained particle seemed somewhat compressed, most likely due to specimen drying.

A thin-stemmed or thick- stemmed mushroom?

The treatment of urothelial plaques with low concentrations of Triton X-100 yielded useful information regarding the orientation of the 16 nm AUM particle, as well as the overall size and shape of its transmembrane moiety. Since the 16 nm AUM particle is highly symmetric when looked at down the hexagonal axis from both sides, it had sometime been difficult to determine the orientation of a particle unambiguously. In the past, we tried to circumvent this problem by modifying the pH or other incubation conditions so that we can manipulate whether AUM plaques are bound to the EM grid *via* their luminal or cytoplasmic surfaces.[9] Alternatively, we deduced that the top of the 16 nm AUM particle could sometimes be flattened as a result of its strong binding to the grid.[9] We show here that the treatment of a biomembrane using low concentrations of Triton X-100 provides a simple method for determining the sidedness of the visualized membrane structure (Figure 2(d) and (e)). Another important aspect of the detergent data has to do with the visualization of the transmembrane moiety. Obviously, the detergent treatment has to be optimized, since too little detergent does not permit the stain to penetrate adequately into the lipid bilayer, while too much detergent results in membrane destruction. Our data have enabled us to visualize some of the transmembrane moieties of the urothelial AUM particle. Interestingly, the maximal diameter of the partially ''uncovered'' transmembrane moiety exhibits an outermost diameter of ~14 nm (Figure 2(e)). This observation is supported by our AFM data, which revealed a similar-sized protrusion on the cytoplasmic surface of urothelial plaques (see Figure 3). The finding that the lateral extent of the transmembrane moiety and of its cytoplasmic protrusion pattern is as large as 14 nm is inconsistent with the earlier quick-freeze/deep-etch studies, which documented that the urothelial AUM particle exhibits a mushroom-like appearance with a large luminal head that is anchored into the lipid bilayer *via* a more slender 11 nm diameter stalk.[5] However, it is well known that the split/etching of a biomembrane can sometimes induce significant plastic deformation of the transmembrane moiety. In the studies of urothelial plaques using the quick-freeze deep-etch technique, for example, one can sometimes observe a significant elongation and concomitant narrowing of the newly exposed ''stalk'' portion of the 16 nm AUM particle.[5] Our current data suggest strongly that the stalk of the AUM particle is actually more massive, with a diameter of about 14 nm, which is only slightly smaller than that of the head.

Association of uroplakin Ia with the six inner domains

Using a chemical cross-linking approach, Wu *et al*. found that UPIa interacts selectively with UPII, and UPIb with UPIII.[17] It was thus proposed that there exist two types of AUM plaques that consist of either UPIa/UPII or UPIb/UPIII, with the UPIs occupying the inner domains and UPII or UPIII occupying the outer domains.[17] However, the calculated molecular mass of six such pairs of UPIa/UPII amounts to only about 250 kDa, which

is much smaller than the 1120 kDa mass of the 16 nm AUM particle determined by scanning transmission EM (STEM).[9] Moreover, it has been shown recently by EM-localization that UPIII is associated with all AUM plaques,[18] making it unlikely that there are two distinct types of plaques. Our present localization data demonstrate that UPIa is associated with the six inner domains of the AUM particle. Taken together, the available data suggest that each basic building block of the 16 nm AUM particle (i.e. consisting of one inner and one outer domain) is composed of all four uroplakins (i.e. one copy each of UPIa, Ib, II and III), with UPIa occupying a part of the inner domain. If so, the total molecular mass of the 16 nm AUM particle (containing six copies of UPIa, UPIb, UPII and UPIII) would amount to about 700 kDa, which is much closer to the estimated 1120 kDa according to Walz *et al*.[9]

Inner AUM particle domain and FimH-induced signal transduction

Our finding that FimH, the high-mannose-binding lectin located at the tip of the type 1 fimbrium, binds to the inner domains of the 16 nm urothelial AUM particle (Figure 5) is interesting in several aspects. First, although we have shown previously that recombinant FimH as well as type 1-fimbriated *E. coli* can bind *in vitro* to SDS-denatured and SDS-PAGE-resolved UPIa, our current data provide the first evidence that the high-mannose sugar moities of the UPIa, even when they are a part of the intact urothelial plaques, are readily available for bacterial binding. This observation is consistent with a recent report, that the tips of the type 1-fimbriated *E. coli* could bind to the center of the individual AUM particles on the apical surface of the urothelium.[8] Second, we have demonstrated recently that FimH binds to its urothelial receptor with only a moderate affinity ($K_d \sim 100$ nM). However, since each 16 nm AUM particle contains multiple bacterial binding sites, there is a great abundance of urothelial surface receptors. This arrangement, in turn, allows each multi-fimbriated bacterium to bind to multiple urothelial sites. The chance that all these bonds will fail simultaneously is small, thereby eliminating the need for high-affinity binding sites which, in fact, may be harmful for the bacteria if they are to survive immunological surveillance.[40] Third, recent data from Hultgren and co-workers indicate that the binding of type 1-fimbriated *E. coli* to the apical urothelial surface can trigger host-cell responses, thus leading to the engulfment of the bacteria, as well as the apoptosis and shedding of the urothelial cells, processes that are important for the innate host defense mechanisms and recurrent urinary tract infection.[8,41] It is therefore important to understand the molecular events triggered by the binding of FimH to its urothelial receptor. Our finding that uroplakin Ia, the FimH receptor, is associated with the inner domains of the 16 nm urothelial AUM particle suggests that these inner domains may play a functional role in this transmembrane signal transduction.

Materials and Methods

Isolation and negative staining of AUM plaques

Bovine and mouse urothelial AUM plaques were isolated by sucrose density-gradient and differential detergent wash.[31,32] For negative staining, 5 μl of the AUM sample (0.1 μg/μl in a storage buffer of 15 mM Hepes-NaOH (pH 7.5), 1 mM EDTA and 1 mM EGTA) was applied to a newly glow-discharged carbon film supported by a copper grid (300-mesh), and the absorbed AUM plaques were then stained using 0.75 % (w/v) uranyl formate (pH 4.25).[9] In some experiments, the storage buffer contained an additional 0.0-0.2 % Triton X-100.

FimH binding to purified mouse AUM

Recombinant FimH/FimC complex was purified by ion-exchange chromatography as described.[24] This complex (0.2 μg/μl in AUM storage buffer) was mixed with an equal volume of purified mouse AUM (0.1 μg/μl) and incubated at room temperature for 40 minutes to three hours. The mixture was absorbed onto a carbon film on a copper grid and stained with uranyl formate (see above).

Image recording and processing

The negatively stained AUM samples were examined using a Philips CM200 FEG transmission EM operated at 200 kV. Micrographs of AUM plaques that were >0.5 μm in diameter were taken in a low-dose mode at a magnification of 50,000×. After the low-dose image was taken, each plaque was examined using a CCD camera to exclude plaques that were folded or double-layered. For 3-D reconstruction, tilted images were taken at 0°, 20°, 30°, 45° and 55°. Since the crystal has P_6 symmetry, tilt angles were done in only one direction. The micrographs were screened using an optical diffraction bench to select the regions that yielded the highest-resolution diffractions (better than 20 Å). The selected micrographs were then scanned using a microdensitometer at a step size of 20 μm, which corresponds to 4 Å in the crystal. After the digitized images were transferred to SGI computers, they were corrected for long-range disorder, merged and used to calculate the averaged projection maps using MRC[42,43] and CCP4[44] software suites. After correction distortion, each image contains 2600 × 2600 pixels and >1000 unit cells. The final 3-D density was displayed using program O.[45] The difference map was calculated according to Kubalek *et al*.[37] The amplitude of both FimH-bound AUM and native AUM were scaled to the same level before they were used for calculating the differences.[37]

Atomic force microscopy

All AFM measurements were performed with a Nanoscope III (Digital Instruments, Santa Barbara, CA) equipped with a 120 μm scanner (*j*-scanner) and a fluid cell. Oxide-sharpened silicon nitride cantilevers with a nominal spring constant of 0.06 N/m from Digital Instruments were used. Before use, the fluid cell was cleaned with normal dish cleaner, followed by ethanol

and finally ultrapure water rinsing. Small disks, ~5 mm in diameter, were punched out of mica (Mica New York Corp., New York) and glued with water-insoluble epoxy glue (Araldite, Ciba Geigy AG, Basel, Switzerland) onto a Teflon disc that, in turn, was supported by a slightly smaller diameter steel disc. The steel disc is required so that the specimen can be mounted magnetically onto the piezoelectric scanner. Sample preparation for AFM was done by placing 2 μl aliquots of isolated AUM onto a freshly cleaved piece of mica. To achieve stable adsorption for imaging the luminal membrane surface, storage buffer (10 mM Hepes-NaOH, pH 7.5) was used. In contrast, when aiming to image the cytoplasmic membrane surface, i.e. to stably adsorb the AUM plaques with their luminal face to the mica surface, we used 10 mM Tris-HCl (pH 8.5), 250 mM KCl. After about 15 minutes of adsorption, the sample was washed gently with the buffer used for imaging (10 mM Hepes (pH 7.5), 250 mM KCl) to remove the non-adsorbing membranes. All AFM imaging was performed in contact mode and at a scan speed of ~5.5 Hz.

Superimposition and alignment of the negative staining and AFM images

Superimposition and visualization of the negatively stained 3-D reconstruction and a luminal surface obtained by AFM was done in ViPEr, a novel platform-independent visual-programming environment based on Python, Tkinter and OpenGL (M.F. Sanner, D.S., & A.J. Olson, unpublished results). Individual software components such as read grid or display surface are connected visually in a graphical network editor to create a computational pipeline.

The electron density map of the 16 nm particle was read into ViPEr using the CCP4 mapin command and displayed as a solid surface using ViPEr indexed polygons.[44] Next, a custom module was written to convert an AFM greyscale TIFF file of the luminal side into a heightfield and to display it as a quad mesh. Symmetry server modules were used to superimpose and align the two geometries in relation to each other.

Acknowledgements

We thank Manfred Auer for his help in using the MRC software package, Juan Lafaille for providing moue bladder tissues, and Bachera Kachar for useful discussions. This work was supported by NIH grants DK52206, DK57269, and DK39753 (to X.P.K. and T.T.S.). In addition, this work was supported by the NCCR Program on ''Nanoscale Science'' of the Swiss National Science Foundation, and by the M.E. Müller Foundation of Switzerland (to U.A.)

References

1. Porter, K. R. & Bonneville, M. A. (1963). *An introduction to the Fine Structure of Cells and Tissues*, Lea and Febiger, New York.
2. Hicks, R. M. (1965). The fine structure of the transitional epithelium of rat ureter. *J. Cell. Biol.* **26**, 25-48.
3. Koss, L. G. (1969). The asymmetric unit membranes of the epithelium of the urinary bladder of the rat. An electron microscopic study of a mechanism of epithelial maturation and function. *Lab. Invest.* **21**, 154-168.
4. Staehelin, L. A., Chlapowski, F. J. & Bonneville, M. A. (1972). Lumenal plasma membrane of the urinary bladder. I. Three-dimensional reconstruction from freeze-etch images. *J. Cell. Biol.* **53**, 73-91.
5. Kachar, B., Liang, F., Lins, U., Ding, M., Wu, X. R., Stoffler, D. *et al*. (1999). Three-dimensional analysis of the 16 nm urothelial plaque particle: luminal surface exposure, preferential head-to-head interaction, and hinge formation. *J. Mol. Biol.* **285**, 595-608.
6. Sun, T. T., Liang, F. X. & Wu, X. R. (1999). Uroplakins as markers of urothelial differentiation. *Advan. Expt. Med. Biol.* **462**, 7-18.
7. Lewis, S. A. (2000). Everything you wanted to know about the bladder epithelium but were afraid to ask. *Am. J. Physiol. Renal. Physiol.* **278**, F867-F874.
8. Mulvey, M. A., Lopez-Boado, Y. S., Wilson, C. L., Roth, R., Parks, W. C., Heuser, J. & Hultgren, S. J. (1998). Induction and evasion of host defenses by type 1-piliated uropathogenic *Escherichia coli*. *Science,* **282**, 1494-1497.
9. Walz, T., Haner, M., Wu, X. R., Henn, C., Engel, A., Sun, T. T. & Aebi, U. (1995). Towards the molecular architecture of the asymmetric unit membrane of the mammalian urinary bladder epithelium: a closed ''twisted ribbon'' structure. *J. Mol. Biol.* **248**, 887-900.
10. Robertson, J. D. & Vergara, J. (1980). Analysis of the structure of intramembrane particles of the mammalian urinary bladder. *J. Cell. Biol.* **86**, 514-528.
11. Maecker, H. T., Todd, S. C. & Levy, S. (1997). The tetraspanin superfamily: molecular facilitators. *FASEB J.* **11**, 428-442.
12. Boucheix, C. & Rubinstein, E. (2001). Tetraspanins. *Cell. Mol. Life Sci.* **58**, 1189-1205.
13. Wu, X. R. & Sun, T. T. (1993). Molecular cloning of a 47 kDa tissue-specific and differentiation-dependent urothelial cell surface glycoprotein. *J. Cell. Sci.* **106**, 31-43.
14. Lin, J. H., Wu, X. R., Kreibich, G. & Sun, T. T. (1994). Precursor sequence, processing, and urothelium-specific expression of a major 15-kDa protein subunit of asymmetric unit membrane. *J. Biol. Chem.* **269**, 1775-1784.
15. Yu, J., Lin, J. H., Wu, X. R. & Sun, T. T. (1994). Uroplakins Ia and Ib, two major differentiation products of bladder epithelium, belong to a family of four transmembrane domain (4TM) proteins. *J. Cell. Biol.* **125**, 171-182.
16. Sun, T. T., Zhao, H., Provet, J., Aebi, U. & Wu, X. R. (1996). Formation of asymmetric unit membrane during urothelial differentiation. *Mol. Biol. Rep.* **23**, 3-11.
17. Wu, X. R., Medina, J. J. & Sun, T. T. (1995). Selective interactions of UPIa and UPIb, two members of the transmembrane 4 superfamily, with distinct single transmembrane-domained proteins in differentiated urothelial cells. *J. Biol. Chem.* **270**, 29752-29759.
18. Liang, F. X., Riedel, I., Deng, F. M., Zhou, G., Xu, C., Wu, X. R. *et al*. (2001). Organization of uroplakin subunits: transmembrane topology, pair formation and plaque composition. *Biochem. J.* **355**, 13-18.
19. Hu, P., Deng, F. M., Liang, F. X., Hu, C. M., Auerbach, A. B., Shapiro, E. *et al*. (2000). Ablation of uroplakin III gene results in small urothelial plaques, urothelial leakage, and vesicoureteral reflux. *J. Cell. Biol.* **151**, 961-972.
20. Zhou, G., Mo, W. J., Min, G. W., Sebbel, P., Neubert, T. A., Glockshuber, R. *et al*. (2001). Uropla-

kin Ia is the urothelial receptor for uropathogenic *Escherichia coli*: evidence from in vitro FimH binding. *J. Cell. Sci.* **114**, 4095-4103.
21. Abraham, S. N., Sun, D., Dale, J. B. & Beachey, E. H. (1988). Conservation of the D-mannose-adhesion protein among type 1 fimbriated members of the family Enterobacteriaceae. *Nature,* **336**, 682-684.
22. Jones, C. H., Pinkner, J. S., Roth, R., Heuser, J., Nicholes, A. V., Abraham, S. N. & Hultgren, S. J. (1995). FimH adhesin of type 1 pili is assembled into a fibrillar tip structure in the Enterobacteriaceae. *Proc. Natl Acad. Sci. USA,* **92**, 2081-2085.
23. Langermann, S., Palaszynski, S., Barnhart, M., Auguste, G., Pinkner, J. S., Burlein, J. *et al.* (1997). Prevention of mucosal *Escherichia coli* infection by FimH-adhesin-based systemic vaccination. *Science,* **276**, 607-611.
24. Pellecchia, M., Sebbel, P., Hermanns, U., Wuthrich, K. & Glockshuber, R. (1999). Pilus chaperone FimC-adhesin FimH interactions mapped by TROSY-NMR. *Nature Struct. Biol.* **6**, 336-339.
25. Aebi, U., Heggeler, B. T., Onorato, L., Kistler, J. & Showe, M. K. (1977). New method for localizing proteins in periodic structures: Fab fragment labeling combinined with image processing of electron micrographs. *Proc. Natl Acad. Sci. USA,* **74**, 5514-5518.
26. Buhle, E. L., Jr & Aebi, U. (1984). Specific labeling of protein domains with antibody fragments. *J. Ultrastruct. Res.* **89**, 165-178.
27. Brisson, A. & Wade, R. H. (1983). Three-dimensional structure of luminal plasma membrane protein from urinary bladder. *J. Mol. Biol.* **166**, 21-36.
28. Taylor, K. A. & Robertson, J. D. (1984). Analysis of the three-dimensional structure of the urinary bladder epithelial cell membranes. *J. Ultrastruct. Res.* **87**, 23-30.
29. Zhang, Z. T., Pak, J., Shapiro, E., Sun, T. T. & Wu, X. R. (1999). Urothelium-specific expression of an oncogene in transgenic mice induced the formation of carcinoma in situ and invasive transitional cell carcinoma. *Cancer Res.* **59**, 3512-3517.
30. Zhang, Z. T., Pak, J., Huang, H. Y., Shapiro, E., Sun, T. T., Pellicer, A. & Wu, X. R. (2001). Role of Ha-ras activation in superficial papillary pathway of urothelial tumor formation. *Oncogene,* **20**, 1973-1980.
31. Wu, X. R., Manabe, M., Yu, J. & Sun, T. T. (1990). Large scale purification and immunolocalization of bovine uroplakins I, II, and III. Molecular markers of urothelial differentiation. *J. Biol. Chem.* **265**, 19170-19179.
32. Liang, F., Kachar, B., Ding, M., Zhai, Z., Wu, X. R. & Sun, T. T. (1999). Urothelial hinge as a highly specialized membrane: detergent-insolubility, urohingin association, and *in vitro* formation. *Differentiation,* **65**, 59-69.
33. Vergara, J., Longley, W. & Robertson, J. D. (1969). A hexagonal arrangement of subunits in membrane of mouse urinary bladder. *J. Mol. Biol.* **46**, 593-596.
34. Warren, R. C. & Hicks, R. M. (1970). Structure of the subunits in the thick luminal membrane of rat urinary bladder. *Nature,* **227**, 280-281.
35. Engel, A., Lyubchenko, Y. & Muller, D. (1999). Atomic force microscopy: a powerful tool to observe biomolecules at work. *Trends Cell Biol.* **9**, 77-80.
36. Choudhury, D., Thompson, A., Stojanoff, V., Langermann, S., Pinkner, J., Hultgren, S. J. & Knight, S. D. (1999). X-ray structure of the FimC-FimH chaperone-adhesin complex from uropathogenic *Escherichia coli*. *Science,* **285**, 1061-1066.
37. Kubalek, E., Ralston, S., Lindstrom, J. & Unwin, N. (1987). Location of subunits within the acetylcholine receptor by electron image analysis of tubular crystals from *Torpedo marmorata*. *J. Cell. Biol.* **105**, 9-18.
38. Hicks, R. M., Ketterer, B. & Warren, R. C. (1974). The ultrastructure and chemistry of the luminal plasma membrane of the mammalian urinary bladder: a structure with low permeability to water and ions. *Phil. Trans. Roy Soc. ser. B,* **268**, 23-38.
39. Wu, X. R., Lin, J. H., Walz, T., Haner, M., Yu, J., Aebi, U. & Sun, T. T. (1994). Mammalian uroplakins. A group of highly conserved urothelial differentiation-related membrane proteins. *J. Biol. Chem.* **269**, 13716-13724.
40. Beachey, E. H. (1981). Bacterial adherence: adhesin-receptor interactions mediating the attachment of bacteria to mucosal surface. *J. Infect. Dis.* **143**, 325-345.
41. Martinez, J. J., Mulvey, M. A., Schilling, J. D., Pinkner, J. S. & Hultgren, S. J. (2000). Type 1 pilus-mediated bacterial invasion of bladder epithelial cells. *EMBO J.* **19**, 2803-2812.
42. Henderson, R., Baldwin, J. M., Ceska, T. A., Zemlin, F., Beckmann, E. & Downing, K. H. (1990). Model for the structure of bacteriorhodopsin based on high-resolution electron cryo-microscopy. *J. Mol. Biol.* **213**, 899-929.
43. Crowther, R. A., Henderson, R. & Smith, J. M. (1996). MRC image processing programs. *116,,* 9-16.
44. Collaborative Computational Project, Number 4 (1994). The CCP4 suite: programs for protein crystallography. *Acta Crystallog. sect. D,* **50**, 760-763.
45. Jones, T. A., Zou, J. Y., Cowan, S. W. & Kjeldgaard, M. (1991). Improved methods for building protein models in electron density maps and the location of errors in these models. *Acta Crystallog. sect. A,* **47**, 110-119.
46. Agard, D. A. (1983). A least-squares method for determining structure factors in three- dimensional tilted-view reconstructions. *J. Mol. Biol.* **167**, 849-852.

Edited by W. Baumeister

(Received 13 November 2001; received in revised form 7 January 2002; accepted 16 January 2002)